Available online at www.sciencedirect.com
ScienceDirect
Applied Catalysis B: Environmental 80 (2008) 51–61
APPLIED CATALYSIS B: ENVIRONMENTAL
www.elsevier.com/locate/apcatb

Mechanism of stearic acid oxidation over nanocrystalline $La_{1-x}A'_xBO_3$ (A′ = Sr, Ce; B = Co, Mn): The role of oxygen mobility

S. Royer [a], B. Levasseur [b], H. Alamdari [c], J. Barbier Jr. [a,*], D. Duprez [a], S. Kaliaguine [b]

[a] LACCO—UMR CNRS 6503, Université de Poitiers, F-86022 Poitiers Cedex, France
[b] Department of Chemical Engineering, Laval University, Québec G1K 7P4, Canada
[c] Department of Mining, Metallurgy and Materials Engineering, Laval University, Québec G1K 7P4, Canada

Received 22 August 2007; received in revised form 12 November 2007; accepted 17 November 2007
Available online 22 November 2007

Abstract

Catalytic wet air oxidation reaction (CWAO) of stearic acid is carried out in a batch reactor over a series of transition metal-based perovskite samples synthesized by reactive grinding. It is observed that the $LaCoO_3$ sample presents the highest initial activity for this reaction. For comparison, pure and substituted $LaMnO_3$ samples show largely smaller activity in spite of similar specific surface areas. The results show that the accessibility of the low temperature active oxygen (or the reducibility of the transition metal) on the surface of the catalyst conditioned the initial activity of the catalyst. Then, a mechanism involving the reaction of stearic acid molecules with adsorbed oxygen surface site ($Co^{3+}O_2^-$) is proposed on the basis of the experimental results. Stearic acid oxidation proceeds via a recurrent decarboxylation process that results in the reduction of cobalt surface sites and formation of surface carbonate species (CO_3^-). In opposition to what was observed for gas phase oxidation reactions, lanthanum (and Ce or Sr) is found to be massively carbonated during the reaction, leading to the destruction of the perovskite structure and loss of the catalytic activity.

Keywords: Perovskite; Catalytic wet air oxidation; Stearic acid; Catalytic activity; Stability

1. Introduction

Due to more and more drastic environmental restraints, recently developed catalytic wet air oxidation process (CWAO) found legitimacy for application in industrial and urban water depollution. Different treatments can be used for the abatement of the chemical oxygen demand (COD). While for diluted non-toxic pollutants a biological treatment is used, depollution of heavily polluted water is generally performed by incineration. In the case of polluted water presenting an intermediate pollution (COD typically comprised between 5 and 150 $g_{O_2}\,L^{-1}$), the CWAO process appears to be a promising treatment [1]. As a matter of fact, catalytic wet air oxidation reactions were extensively studied over a large variety of homogeneous and heterogeneous catalysts. Phenol oxidation reaction was studied over Al_2O_3 supported CuO–ZnO [2], noble metal on CeO_2 [3,4] and mixed Mn–Ce oxides [5–7]. On the other hand, oxidation of carboxylic acids was also reported on noble metal supported on CeO_2 [8–11]. The catalyst is then used to oxidize (or mineralize) the organic contaminants into CO_2 and H_2O, or to convert toxic pollutants into non-toxic or biodegradable compounds. Nevertheless, CWAO reaction is based on the use of O_2 (or air) as oxidant, which requires more severe operating conditions (high temperature and high oxygen pressure) than ozone or hydrogen peroxide.

To our knowledge, the activity of transition metal-based mixed oxides in wet air oxidation reaction such as carboxylic acids CWAO has rarely been studied. However, some mixed oxides, and especially transition metal-based perovskites (of general formula ABO_3), are known to show interesting activities in gas phase oxidation reactions [12–14]. Some authors reported comparable activities between perovkites and noble metal supported catalysts for some oxidation reactions [15]. Among a wide range of compositions (perovskite structure can be achieved when the tolerance factor, $t = (r_A + r_O)/\sqrt{2}(r_B + r_O)$, lies between 0.75 and 1), cobalt and manganese-based perovskites are found to be the most active. As such, systems with lanthanum in A position, and

* Corresponding author. Tel.: +33 5 49 45 48 31; fax: +33 5 49 45 34 99.
E-mail address: jacques.barbier.jr@univ-poitiers.fr (J. Barbier Jr.).

0926-3373/$ – see front matter © 2007 Elsevier B.V. All rights reserved.
doi:10.1016/j.apcatb.2007.11.012

cobalt or manganese in B position, are the most studied perovskite systems [16–18] in gas phase oxidation reactions. Much more efforts were also made in order to increase activity by partial substitution of the A cation by cations of different valencies, such as Ce^{4+} or Sr^{2+} [19–21]. These substitutions were suggested to modify the concentration of the oxygen vacancies on the surface and in the bulk of perovskites. Moreover, the mean transition metal valency (Co^{3+}/Co^{2+} or Mn^{4+}/Mn^{3+}) and the oxygen mobility seem to be strongly influenced by these substitutions, which could partially explain the differences observed in terms of oxidation catalytic activity. To our knowledge, only one recent study deals with the activity of $LaFeO_3$ sample for the CWAO of phenol, benzoic acid, salicylic acid and sulfonic salicylic acid [22]. Authors claim a high activity and high stability of the $LaFeO_3$ catalysts, especially for the oxidation of salicylic acid.

In this work, four perovskite samples were tested for wet air oxidation reaction of stearic acid. Stearic acid is the most common saturated fatty acid present in the animal fats [23] and is choose as model molecule for this study. Reactions were performed in a batch reactor, and results were compared to those obtained for ceria supported noble metal catalysts [11]. Since the mechanism of oxidation on perovskite is suggested to involve oxygen mobility (or transition metal reducibility), surface oxygen reactivity, obtained by oxygen storage capacity measurement, is compared to the activities obtained for the reaction. Each sample was characterized before and after test by X-ray diffraction, elementary analysis, N_2 adsorption–desorption, and oxygen storage capacity (OSC) to evaluate the stability under the experimental test conditions.

2. Experimental

2.1. Catalyst synthesis

Four perovskites of different compositions ($LaCoO_3$, $LaMnO_3$, $La_{0.6}Sr_{0.4}MnO_3$ and $La_{0.9}Ce_{0.1}MnO_3$) (Table 1) were studied. Reactive grinding is an original method developed and patented at Laval University [24–26]. Compared to conventional methods, such as citrate coprecipitation [27] and citric acid complexation [28], perovskite crystallization in this method occurs near ambient temperature by replacing the thermal energy necessary for the crystallization, by mechanical grinding energy. Thus, larger specific surface areas and smaller crystal domain sizes are obtained by this method compared to those obtained by other conventional methods [29]. The synthesis of the samples used in this work was fully described in a previous work [30], and is only briefly summarized here.

Table 1
Physical and redox properties of the studied samples

Sample	Formula	S_{BET} ($m^2\ g^{-1}$)	OSC[a] ($\mu mol\ g^{-1}$)	ξ in ABO_ξ[b]
LaCo	$LaCoO_3$	50.4	194	2.95
LaMn	$LaMnO_{3+\delta}$	55.8	45	3.13
LaSrMn	$La_{0.6}Mn_{0.4}O_{3+\delta}$	47.9	52	3.13
LaCeMn	$La_{0.9}Ce_{0.1}O_{3+\delta}$	66.8	40	3.14

[a] OSC is the total amount of CO consumed per gram of catalyst, during the first CO pulse of the alternate series (step 4).

[b] Oxygen stoichiometry in ABO_ξ, calculated from the OSC value, assuming an initial oxygen stoichiometry of 3.00 for LaCo and 3.15 for Mn-based samples.

The oxide precursors were first calcined in a muffle furnace and introduced in a stainless steel vial with stainless steel balls. The sample was ground for 4 h. Perovskite crystallization is achieved at the end of this step. The resulting powder was mixed to equivalent quantity of ZnO powder and ground a second time for 20 h. The obtained powder mixture (perovskite + ZnO) was washed repeatedly with diluted ammonium chloride and water in order to remove the ZnO (less than 0.5 wt% of ZnO in the solid after washing).

2.2. Physical characterization

XRD patterns of the samples, before and after the oxidation test, were recorded using a SIEMENS D5000 diffractometer with a Cu Kα radiation as X-ray source ($\lambda = 1.54056$ Å). Spectra were spanning 2θ values comprised between 15° and 75° using 2.4 s collection time for each 0.05° step. Phase identification was made by comparison with JCPDS files.

Specific surface areas were obtained from N_2 adsorption at −196 °C, using an OMNISORP 100 apparatus. About 0.5 g of catalyst was first evacuated for 6 h at 200 °C. The specific surface area was calculated from the linear part of the BET line.

The amount of carbon deposited on the catalyst after test was quantified using a C, H, N analyzer NA2100 from C.E. Instruments. Amounts of cobalt, manganese and lanthanum lixiviated during reaction were evaluated by ICP analysis of the reaction medium using a PerkinElmer Optima 2000 D.

2.3. OSC measurements

OSC setup and data treatment were fully described in Ref. [30] and will only be briefly summarized below. OSC measurements were performed in a pulsed U-shaped microreactor. The OSC measurement comprised four successive steps (one pulse = 10.9 μmol of gas):

1. O_2 pulses for saturation of the catalyst.
2. CO pulses, until zero consumption of CO.
3. O_2 pulses for reoxidation of the solid.
4. Alternated pulses CO–O_2–CO–O_2–CO–O_2.

Reactant and products analyses were performed using a gas chromatograph equipped with a TCD and a Porapak Q type column (i.d. = (1/4) in., $L = 0.5$ m).

The oxygen storage capacity (OSC values in Table 1) is calculated from the amount of CO consumed during the first CO pulse from the alternated series (step 4) at 180 °C. This value corresponds to the amount of highly active oxygen, which is immediately available for the reaction at the temperature of test.

In the case of the lanthanum cobalt perovskite, cobalt is mainly trivalent [29,31–33], with a general formula close to $LaCoO_3$. For lanthanum manganese-based perovskite, some

authors [34–36] reported that an important fraction of the manganese is in the 4+ valency. Thus, the oxygen stoichiometry (ξ, Table 1) can be calculated from the oxygen balance using Eqs. (1) (for $LaCoO_3$) and (2) (for manganese-based samples):

$$R(\%) = 100 \times \frac{3-\xi}{0.5} \quad (1)$$

$$R(\%) = 100 \times \frac{3.15-\xi}{0.15} \quad (2)$$

with R is the reduction degree of the transition metal.

2.4. Stearic acid oxidation reaction

Stearic acid wet air oxidation reaction was performed in a 440 mL Hastelloy C22 autoclave. The experimental setup is schematized Fig. 1. Stearic acid ($C_{18}H_{34}O_2$, 0.9 g) in the form of white flakes was added to 160 mL of double purified water. A 0.640 g of catalyst (4 $g_{cata}\,L^{-1}$) was added to the mixture, and the autoclave hermetically closed and purged under helium at room temperature. The temperature of the autoclave was then raised up to 200 °C (ramp = 2.5 °C min^{-1}) under stirring (agitation speed = 250 rpm, no diffusional resistance occurs under these conditions). The reaction started as soon as the O_2 pressure inside the autoclave was increased to 2 MPa. The O_2 pressure was maintained constant at this value over the 180 min testing time. As the complete oxidation of stearic acid requires 26 mol O_2/mol of stearic acid (Eq. (3)), and because of the low solubility of O_2 in water at 200 °C [36] ($O_2 < 10^{-1}$ mol L^{-1} at 200 °C), stearic acid always remains in excess with respect to oxygen during the test.

$$C_{18}H_{34}O_2 + 26O_2 \rightarrow 18CO_2 + 18H_2O \quad (3)$$

Gas phase analysis was performed using a gas chromatograph Intersmat IGC120ML, equipped with a catharometer for quantification (carrier gas = He), and a Porapak Q packed column (i.d. = 0.6 mm, L = 0.5 m) for separation of He, O_2 and CO_2. Knowing CO_2 concentration in the gas phase, it is possible from the experimental calibration curves obtained at different temperatures (see Ref. [37]), to calculate the total CO_2 content in the reactor (gas + liquid). The mineralization molar ratio (M), defined as the molar ratio between the amount of CO_2 produced and the initial amount of organic carbon introduced as stearic acid ($[Stearic]_i$), can be calculated using the following equation:

$$M = \frac{CO_2}{[Stearic]_i} \quad (4)$$

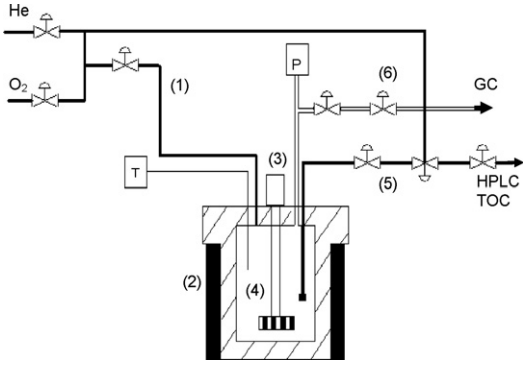

Fig. 1. Experimental setup used for the stearic acid wet air oxidation reaction. (1) Inlet gas, (2) heater, (3) stirrer, (4) reactor, (5) liquid sample, (6) gas sampler. T: thermocouple; P: pressure indicator.

Liquid samples, collected at different reaction times were analyzed to determine:

- *Total organic carbon (TOC) in solution*. Samples initially filtered were diluted in ultra pure water (1/10), and analyzed on a O.I. Analytica analyzer model 1020A. The acetic acid content was subtracted to yield the TOC values reported in Table 2.
- *Acetic acid concentration*. The samples are analyzed by HPLC. Organic compounds are separated at 30 °C in aqueous H_2SO_4 (0.004 N) on an organic acid analysis column Aminex HPX-87H (300 mm × 7.8 mm), and analyzed using a diode array UV–vis detector (UV6000LP from Thermofinnigan) coupled with a refractive index detector (RI-150, Thermofinnigan).

After test, the catalyst was recovered by filtration, and analyzed using the same methods as for the fresh catalysts. Carbon balance (B_c) is defined as the sum of the TOC (total organic carbon in solution as presented Table 2), acetic acid, the carbon in experimentally measured CO_2 (used in calculating mineralization ratio (M)), and the amount of carbon left over the catalyst after the test.

The initial rate of mineralization (mol of CO_2 produced per minute and per gram of catalyst) is calculated using the following equation:

$$r_0 = \frac{M \times 18 \times m_{Stea.Ac.}}{100 \times MW \times t \times m_{catal.}}$$

where t is the time of reaction, M the mineralization degree (%) at t, $m_{Stear.Ac.}$ the mass of stearic acid initially added to the reactor, MW the molecular weight of stearic acid, and $m_{catal.}$ is the mass of catalyst introduced in the reactor.

For manganese-based samples, r_0 is calculated using mineralization measured after 15 min of reaction. For LaCo sample, r_0 is calculated on the conversion obtained after 2 min of reaction since conversion only slightly increased after this time.

Remark: results obtained in this work showed that catalysts deactivated in reaction. Thus, the value of initial rate of mineralization calculated using equation presented above is underestimated. It is however not possible to quantify the decrease in reaction rate due to deactivation for each catalysts.

3. Results

3.1. Physical characterization

Four samples of different compositions were synthesized by reactive grinding: $LaCoO_3$ (LaCo), $LaMnO_3$ (LaMn),

Table 2
Results of the CWAO reaction of stearic acid at 200 °C obtained on the perovskite-type samples

Sample	M[a] (%)	TOC[b] (%)	Acetic acid (%)	Adsorbed carbon[c] (%)	B_c[d] (%)	r_0[e] ($\times 10^{-4}$ mol min^{-1} g^{-1})
LaCo	65.2	11.3	4.5	12.1	93.1	173.4
LaMn	60.2	16.6	8.0	2.7	87.5	14.8
LaSrMn	66.0	–	–	–	–	19.3
LaCeMn	58.6	–	–	–	–	10.5
5% Ru/CeO_2 [11]	74.4	6.3	19.3	0.0	100	6.4

Comparison with Ru/CeO_2 catalyst. Results obtained after 180 min reaction. Values of a, b, c, d and acetic acid are expressed in carbon% of the carbon introduced as stearic acid.
[a] Mineralization degree of stearic acid into CO_2.
[b] Total organic carbon minus the acetic acid.
[c] Amount of carbon left on the used perovskite samples.
[d] Total carbon balance (sum of the mineralization, TOC including acetic acid, and adsorbed carbon).
[e] Initial reaction rate (measured over the first 15 min except for LaCo for which r_0 is measured over the first 2 min of reaction).

$La_{0.6}Sr_{0.4}MnO_3$ (LaSrMn) and $La_{0.9}Ce_{0.1}MnO_3$ (LaCeMn). Complete characterization of the solids was already presented Ref. [30] and we only briefly summarized main physical and structural characteristics of the samples in this part. First, XRD analysis shows almost complete crystallization of the precursors into the perovskite structures. For LaCo, a weak peak attributed to Co_3O_4 is also observed. Some impurities like La_2O_3 (LaMn sample) or SrO (LaSrMn sample) can also be seen in small amount. Specific surface areas are found to vary between 49.7 $m^2\,g^{-1}$ for LaSrMn, and 66.8 $m^2\,g^{-1}$ for LaCeMn (Table 1), that is relatively higher than the specific surface areas reported for samples synthesized by conventional methods (at calcination temperatures between 600 °C and 1000 °C depending on the synthesis procedure) [29,38].

Since the grinding method results usually in some iron contamination [25,29,39], EDX analysis was performed on the LaCo and LaMn samples in order to determine the iron contamination here. Whereas no Fe can be observed on the LaCo sample, EDX gives a Fe/Mn ratio of 0.064 for the LaMn sample which corresponds to a general formula of $La_{0.8}Sr_{0.2}Mn_{0.95}Fe_{0.05}O_3$. Because of the same conditions of grinding for all the samples, similar degree of contamination ($0 < x < 0.05$, in $LaB_{1-x}Fe_xO_3$) is assumed for all the samples.

3.2. OSC measurements

The four samples were calcined at 200 °C and tested for oxygen storage capacity (OSC) at 180 °C. This method was found to be suitable to quantify the amount of oxygen available for reaction at a given temperature [30]. Comparing results obtained by hydrogen temperature programmed reduction (TPR-H_2) and by OSC [30], OSC experiments conducted with $LaCoO_3$ perovskite showed some CO conversion from 180 °C, whereas no reduction can be detected by TPR-H_2 on the same samples until 200 °C. It was therefore possible to perform a precise measurement of some active surface oxygen species of the solids that are not sensed by TPR-H_2. Because of the more precise results obtained by OSC in the low temperature range, this method was preferred to the TPR-H_2 method to determine the amount of reactive oxygen at the temperature of CWAO reaction. These amounts will be directly related to catalytic results. Results obtained in terms of surface reactivity (OSC) were already published [30], and are summarized in Table 1.

3.2.1. $LaCoO_3$ reducibility

The reduction of $LaCoO_3$-type perovskite is known to occur in two successive steps [29–32]. The first reduction step consists in the reduction of the Co^{3+} into Co^{2+} and occurs at low temperature (<550 °C). The second reduction process (reduction of the Co^{2+} into metallic cobalt) starts at temperatures higher than 600 °C [29]. The OSC results obtained for the LaCo sample are summarized in Table 1. At 180 °C, the amount of active oxygen (OSC value) is related to the reduction mechanism described by Eq. (5), where only surface and/or subsurface oxygens are active for reduction. Reoxydation process (Eq. (6)) however takes place at a higher rate.

$$Co_{(surf)}{}^{3+} + CO \rightarrow Co_{(surf)}{}^{2+} + CO_2 \quad \text{(slow)} \tag{5}$$

$$Co_{(surf)}{}^{2+} + \tfrac{1}{2}O_2 \rightarrow Co_{(surf)}{}^{3+} \quad \text{(fast)} \tag{6}$$

3.2.2. $LaMnO_{3.15}$ reducibility

As in the case of the $LaCoO_3$ sample, $LaMnO_{3.15}$ reduction proceeds in two steps [33,40,41]. The first reduction peak is generally attributed to the reduction of all the Mn^{4+} cations initially present in the perovskite structure [30,44,45], together with possible reduction of some Mn^{3+} from the surface of the solid [30]. During the second reduction process (above 600 °C), trivalent manganese is reduced into divalent manganese. The OSC experiment on LaMn showed very limited oxygen storage capacity at 180 °C, in comparison with the LaCo sample [30]. An OSC value of 45 μmol g^{-1} (Table 1) was obtained for LaMn. Thus, OSC obtained at 180 °C can be attributed to the reduction of some surface and subsurface Mn^{4+} into Mn^{3+} [30], as described in the following equation:

$$Mn_{(surf)}{}^{4+} + CO \rightarrow Mn_{(surf)}{}^{3+} + CO_2 \quad \text{(slow, partial)} \tag{7}$$

$$Mn_{(surf)}{}^{3+} + \tfrac{1}{2}O_2 \rightarrow Mn_{(surf)}{}^{4+} \quad \text{(fast)} \tag{8}$$

As observed for $LaCoO_3$, manganese reoxidation proceed at a higher rate (Eq. (8)).

3.2.3. Effect of the lanthanum substitution on the manganese reducibility

OSC results obtained for the Sr (LaSrMn) and Ce (LaCeMn) substituted samples showed slight differences from those obtained for the pure LaMn sample. A slight increase in CO conversion was observed during the first CO pulse of the alternate series (OSC) on the LaSrMn sample. The differences observed during the first CO pulse (quantification of the most active manganese) are attributed to an increase of the Mn^{4+}/Mn^{3+} ratio which takes place to compensate the electric charge of perovskite and compensate the charge effect of Sr^{2+} doping. The cerium substitution results in a slight decrease of the OSC value (40 μmol g^{-1} is then obtained for LaCeMn, Table 1). Then, the decrease in OSC value observed in our work suggests some decrease in manganese reducibility which differs from the results available in the literature [38,42]. In conclusion, neither the amount of low temperature active oxygen, nor the transition metal reducibility, is strongly affected by the strontium or cerium substitution.

3.3. Catalytic wet oxidation reaction

3.3.1. Catalytic activity

The samples were tested in a batch reactor (Fig. 1) for catalytic wet air oxidation reaction of stearic acid. Tests were performed at 200 °C under 2 MPa oxygen pressure. The catalytic results are summarized in Table 2. The mineralization curve obtained for the LaCo sample shows two distinct parts (Fig. 2A). Mineralization quickly increases up to 63% (after 15 min), and then stabilizes around 65% of mineralization. Results obtained for this sample are compared to those obtained under the same conditions with two supported noble metal samples already reported in Ref. [11]. Adding LaCo perovskite in the reactor results in a net increase in CO_2 production (or mineralization) with respect to the blank experiment free of catalyst. The highest initial reaction rate is obtained with the LaCo sample, compared to the 5% Ru/CeO_2 and 5% Pt/CeO_2 samples. An initial reaction rate of 173.4×10^{-4} mol min^{-1} g^{-1} is obtained for the LaCo sample (Table 2), yielding a quick raise of the mineralization degree over a short time (2 min). For sake of comparison, the initial reaction rate obtained for the 5% Ru/CeO_2 samples is 6.4×10^{-4} mol min^{-1} g^{-1} within the first 15 min of reaction, which is 27 times smaller than for LaCo. While a constant mineralization is reached after only 15 min of reaction for LaCo, the mineralization continuously increases with reaction time for the two noble metal-based catalysts (Fig. 2A). This result suggests a quick deactivation of the LaCo sample. Even if the LaCo sample presents the highest initial activity, the catalytic activity after 180 min of reaction is in the order: 5% Pt/CeO_2 (96%) > 5% Ru/CeO_2 (74%) > LaCo (65%).

Fig. 2B presents the results of mineralization obtained for the three manganese-based samples. Slight differences can be seen between the manganese-based samples and the LaCo sample. Mineralization curves obtained on the manganese-based perovskites can also be divided into two parts. The first part is characterized by a quick increase in mineralization degree during the first thirty minutes. However, this rate is

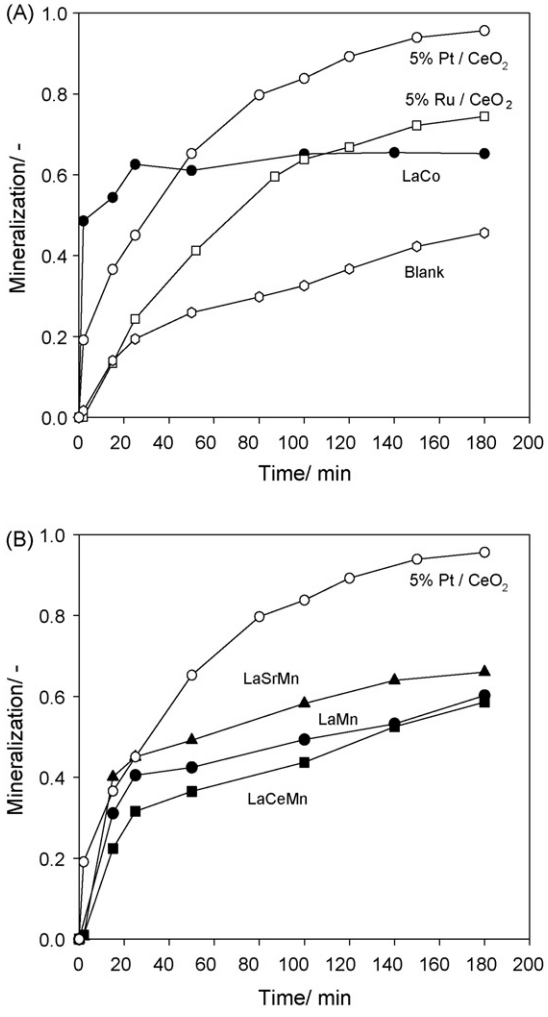

Fig. 2. Mineralization of stearic acid as a function of time at 200 °C over: (A) LaCo; (B) Mn-based samples; comparison with 5% Ru/CeO_2 and 5% Pt/CeO_2 [11].

lower than that of for the LaCo sample (Table 2). The most active manganese-based sample, LaSrMn, showed an initial reaction rate of 19.3×10^{-4} mol min^{-1} g^{-1}, which is nine times lower than that of LaCo (173.4×10^{-4} mol min^{-1} g^{-1}). The reaction rate increases therefore as follows: LaCo ≫ LaSrMn > LaMn > LaCeMn. The Mn-based samples showed initial activities comprised between those of the 5% Pt/CeO_2 and 5% Ru/CeO_2 samples. During the second part of the mineralization curve (between 25 min and 180 min), mineralization is found to linearly increase with reaction time. This slightly differs from the results obtained for the LaCo sample, since a constant value of 65% of mineralization is attained after only 25 min with this sample. In the case of the LaMn sample, mineralization continues to slowly increase from 40.5% after 25 min to 60.2% after 180 min. Similar trends are obtained for LaSrMn and LaCeMn, for which mineralization increases from 45% to 66% and 31.6% to 58.6%, respectively. A significant difference between slopes of the first and second parts of the mineralization curves suggests a partial surface and/or bulk poisoning of Mn-based samples. The degree of poisoning, however, seems to be smaller compared to that of the

LaCo sample since the mineralization process continues until the end of the test.

The evolutions of the carbon balance, defined as the sum of the gas phase as well as dissolved CO_2, and organic carbon in solution (including acetic acid), obtained for the LaCo and LaMn samples are presented in Fig. 3. On this figure, the amounts of carbon adsorbed on the catalyst, as well as the non-soluble carbon in suspension (i.e. non-converted stearic acid) are not quantified. For the LaCo and LaMn samples, the 100% carbon balance is not reached, even after 180 min of reaction. In addition to the CO_2 generated due to mineralization, some organic compounds, and to a lesser extend acetic acid, are also detected in solution (Table 2). Adding the amount of carbon adsorbed on the catalyst (obtained by carbon analysis on the used samples) leads to a carbon balance of 93.1% for LaCo and 87.5% for LaMn. These results suggest that part of the initial stearic acid remains unconverted at the end of the test (12.5% for LaMn). For comparison, the 100% carbon balance is obtained after only 90 min on the 5%Ru/CeO_2 catalyst (Fig. 3). Moreover, the amount of carbon adsorbed on the surface of this catalyst is near 0 at the end of the test. Nevertheless, the mineralization remains incomplete even at the end of the test, and a significant amount of the stearic acid is converted into soluble organic compounds and acetic acid (light and dark grey bars, Fig. 3).

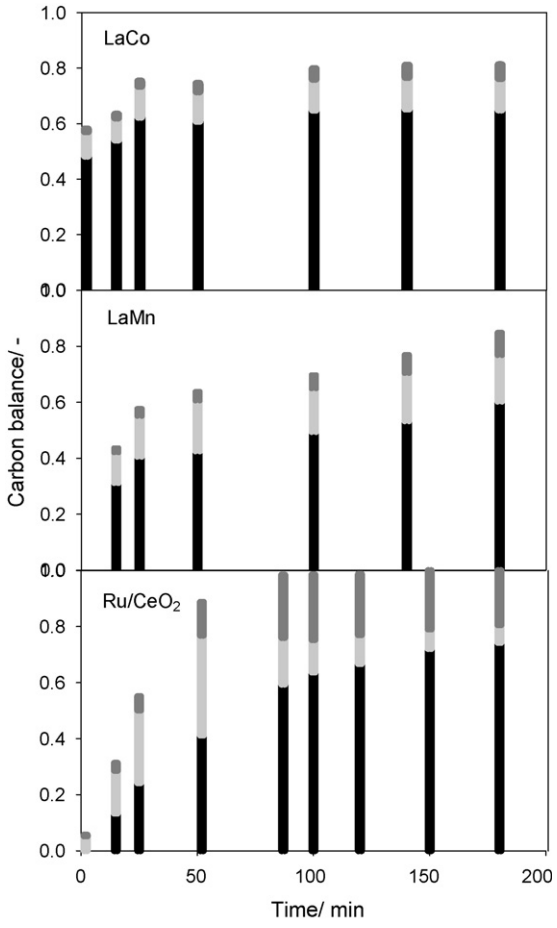

Fig. 3. Evolution of the carbon balance obtained for the LaCo and LaMn samples with reaction time. Comparison with the 5% Ru/CeO_2. Black: mineralization molar ratio; light grey: TOC (except acetic acid); dark grey: acetic acid. Adsorbed carbon is not include in this figure.

3.3.2. Catalyst stability

After test, the catalyst was recovered by filtration, and the specific surface area was measured by N_2 adsorption after drying at 200 °C. The physical properties of the used samples are summarized in Table 3. It was observed that the specific surface area remains almost unchanged after test for both LaCo and LaMn samples. The small differences (between 1.7% and 7.3%) measured for all the samples are within instrumental error. This result strongly differs from those obtained for the noble metal-based catalysts [11]. For example, the specific surface area of 5% Ru/CeO_2 decreased from 226 $m^2\,g^{-1}$ to 87 $m^2\,g^{-1}$ under the same conditions. The significant decrease in specific surface area observed for the noble metal samples were attributed to the sintering process occurring on nanoscale ceria particles. However, there is no evidence of sintering of the noble metal particles as measured by H_2 chemisorption. This indicates that the active phase itself is not deactivated under the test conditions.

The carbon analysis, performed on the used samples, showed strong carbon accumulation of 12.1 wt% on the LaCo sample (Table 2). If the whole lanthanum was in the carbonate form, the total carbon content would be only 5.8 wt%. The excess carbon is therefore attributed to some other carbon species which remain adsorbed on the surface of this solid. Compared to the LaCo sample, the amount of carbon accumulated on the catalyst after test remains rather low ranging from 1.9 wt% (LaCeMn) and 3.2 wt% (LaSrMn). The amount of carbon accumulated on the solid allows to calculate lanthanum carbonation which is comprised between 33% and 49%.

It is also observed that part of the transition metal is partially leached out during the reaction. The amount of transition metal leached out, measured by ICP analysis of the reaction liquid, is presented in Table 3 (TM_{sol}). The amounts of dissolved cobalt and manganese remain low (less than 5% of the initial amount of transition metal introduced in the reactor). At the end of the test, drastic structural changes of the LaCo sample are observed by XRD (Fig. 4). While the fresh sample presents almost a pure rhombohedral $LaCoO_3$ structure, no reflexion attributed to this phase can be detected in the XRD pattern of the used sample (Fig. 4a). After test, the solid is composed of two different compounds: lanthanum carbonate hydroxide hydrate $La(CO_3)_2(OH)\cdot H_2O$ (JCPDS file 029-0387), and cobalt oxide Co_3O_4 (JCPDS file 42-1467). As suggested by the carbon content analysis, all the lanthanum is carbonated at the end of the reaction (Table 3) while some additional carbon is adsorbed on the surface of the solid in an undefined form. Similar diffraction peaks were obtained for the Mn-based samples (Fig. 4b–d). The amount of accumulated carbon is however relatively low compared to that of the LaCo sample (carbon concentration between 1.9 wt% and 3.2 wt%, Table 3). The calculated degree of lanthanum carbonation is then lower compared to LaCo (from 33% for LaCeMn to 49% for LaSrMn). XRD patterns mainly showed diffraction peaks attributed to the initial rhombohedral $LaMnO_{3.15}$ structure.

Table 3
Physical properties of the used samples

Sample	S_{BET} ($m^2\ g^{-1}$)	[C][a] (wt%)	Crystallographic phases[b]	Carbonation degree[c]	OSC[d] ($\mu mol\ g^{-1}$)	TM_{sol}[e] (%)
LaCo	53.0	12.1	Traces P, mainly C and M	100% + adsorbed carbon species	45	3.8
LaMn	56.7	2.7	P, traces C and M	47%	16	4.8
LaSrMn	51.4	3.2	P, traces C and M	49%	–	–
LaCeMn	63.2	1.9	P, traces C and M	33%	–	–

[a] Carbon accumulated on the catalyst after 180 min reaction, as measured by CHN analysis.
[b] Crystallographic phase identified by XRD on the used samples: P, perovskite; LaC, lanthanum carbonate hydroxide hydrate; M, cobalt or manganese oxide.
[c] Formula calculated from the carbon accumulated in the sample, and assuming all the carbon is under the form of lanthanum carbonate.
[d] OSC (immediate reduction) values obtained on the used sample under the same experimental conditions than for the fresh samples.
[e] Lixiviated transition metal in percent of the initial amount of transition metal in the perovskite.

Minor diffraction peaks attributed to the $La(CO_3)_2(OH)\cdot H_2O$ phase (JCPDS file 29-0384) were also recorded but no additional peaks attributed to manganese oxide can be observed. These results suggest that an important part of the accumulated carbon remains in the form of surface adsorbed species, and that the degree of lanthanum carbonation (and strontium or cerium) reported in Table 3 is therefore overestimated. The structural transformations observed by XRD can be therefore associated to the reaction between the initial sample and adsorbed CO_2:

$$6LaCoO_3 + 12CO_{2(ads)} + 2.5O_2 + 3H_2O \rightarrow 6La(CO_3)_2OH\cdot H_2O + 2Co_3O_4 \quad (9)$$

A similar reaction may proceed with the manganese-based perovskites, but with a lower conversion of the solid into lanthanum carbonate hydroxide hydrate and manganese oxide.

The OSC values obtained for the used catalysts (Table 3) are significantly lower than those obtained with the fresh samples (Table 1). The OSC value for the LaCo sample decreases down to 45 $\mu mol\ g^{-1}$, which is 4.3 times lower than that for the fresh sample (194 $\mu mol\ g^{-1}$). Similar result is obtained for the LaMn sample, for which the OSC decreases from 45 $\mu mol\ g^{-1}$ to 16 $\mu mol\ g^{-1}$. Then, the reaction results in a decrease of immediate reducibility of the transition metal. Such a decrease in reducibility can explain why the samples present mineralization curves in two parts (Fig. 2A and B): actually, high initial activity is recorded when all transition metal is active (high OSC). The activity or mineralization rate is then decreased when the reducibility of the transition metal is altered due to carbonation (low OSC) and partial transition metal surface dissolution.

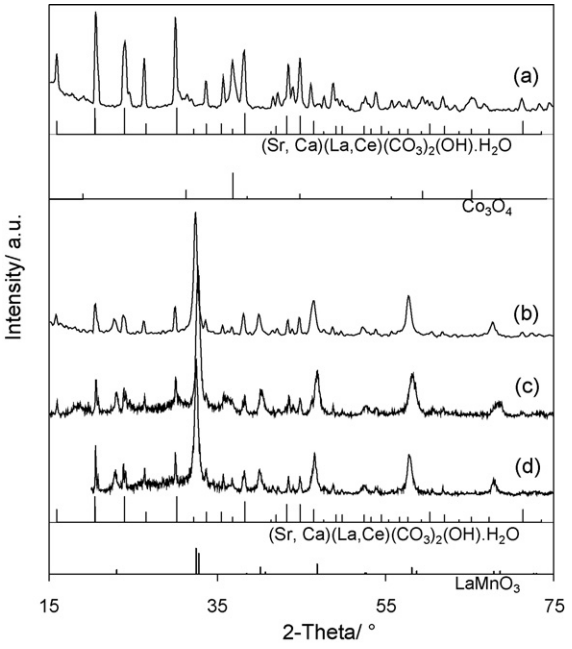

Fig. 4. XRD patterns of the samples after 180 min of reaction. (a) LaCo; (b) LaMn; (c) LaSrMn; (d) LaCeMn.

4. Discussion

4.1. Mechanism of stearic acid oxidation

The mineralization curves show high initial activity for the stearic acid CWAO reaction (see Fig. 2). According to the literature, different mechanisms of oxidation can happen, depending on the rate of acetic acid and other soluble organic compounds formation [11]. In the case of the perovskite samples, the amounts of acetic acid in solution are low in comparison with those obtained for 5% Ru/CeO_2. Moreover, the ratio of dissolved carbon ([TOC + acetic acid]/[stearic]$_i$) (Fig. 5) increases progressively with the time of reaction for the

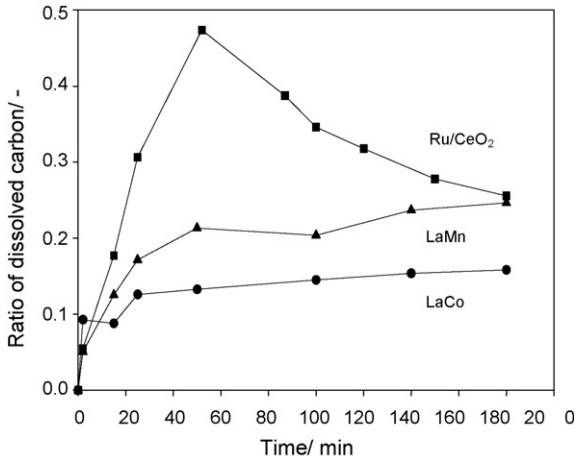

Fig. 5. Ratio of dissolved carbon (defined as [TOC + Acetic acid]/[Stearic]$_i$) obtained for the LaCo and LaMn samples as a function of the time in reaction.

two samples (up to 0.16 for LaCo and 0.24 for LaMn) but remains low (<25%) and comparable to those obtained for the 5% Pt/CeO_2 (11%) and 5% Pd/CeO_2 (17%) (not shown, see [11]). The shape of the curve obtained with the 5% Ru/CeO_2 sample strongly differs from those obtained for the perovskite samples (Fig. 5). The ratio of dissolved carbon quickly increases up to a maximum around 48%, and then slowly decreases with reaction time [11]. The first increase is characteristic of the formation of soluble short-chain carboxylic acids (as measured by the TOC) that are formed by C–C bond rupture, followed by desorption of these products because of an adsorption competition between the stearic acid molecules and the short-chain carboxylic acids. The decrease in stearic acid concentration leads to a progressive consumption of the soluble carboxylic acids to form acetic acid and CO_2. Results obtained for the perovskite samples, which are similar to those obtained for Pd and Pt supported samples and reported in the literature [11], where maxima are not observed (Fig. 5) suggest mainly a direct oxidation process of the stearic acid into CO_2 and CH_3COOH before desorption (recurrent decarboxylation process [43]). According to the mechanism proposed by Sève and Antonini [43] that describes a recurrent decarboxylation path for the wet air oxidation of saturated fatty acids, a molecule of stearic acid will produce 1 molecule of acetic acid and 16 molecules of carbon dioxide. Eqs. (10) (first step) and (11) (final step) summarize the first and last step of the decarboxylation process:

$$C_{17}H_{35}\text{-}COOH + 1.5O_2 \rightarrow C_{16}H_{33}\text{-}COOH + CO_2 + H_2O \quad (10)$$

$$C_2H_5\text{-}COOH + 1.5O_2 \rightarrow CH_3\text{-}COOH + CO_2 + H_2O \quad (11)$$

A pure decarboxylation process leads therefore to a $[CO_2]/[CH_3COOH]$ ratio of 16 and asymptotically reaching this value at high reaction time, and a $[TOC + CH_3COOH]/[CH_3COOH]$ ratio reaching 1 since acetic acid is essentially the only final organic product of the reaction. Evolution of the $[CO_2]/[CH_3COOH]$ and $[TOC + CH_3COOH]/[CH_3COOH]$ ratios with reaction time are given Fig. 6A and B. The $[CO_2]/[CH_3COOH]$ ratio obtained for the LaCo sample is always higher than 16, while that obtained for the LaMn sample decreases from 20.5 to 7.5 (Fig. 6A). However, a $[TOC + CH_3COOH]/[CH_3COOH]$ ratio higher than 1 is always obtained for the two samples (Fig. 6B).

All these results show that CO_2 is the main final product of the reaction in the case of the LaCo sample. A ratio of $[CO_2]/[CH_3COOH]$ largely higher than 16 indicates a low content of acetic acid which can be obtained either by partial oxidation of stearic acid or by secondary oxidation of CH_3COOH. The ratio $[TOC + CH_3COOH]/[CH_3COOH]$ being higher than one (Fig. 6) indicates that the first explanation is more likely. In Ref. [11] the presence of soluble short chain carboxylic acids in the reaction medium was proposed to be associated with the thermal (non-catalytic) oxidation of stearic acid, a process responsible for the rather large solubilization observed during blank (no catalyst present) experiments (see Fig. 2A).

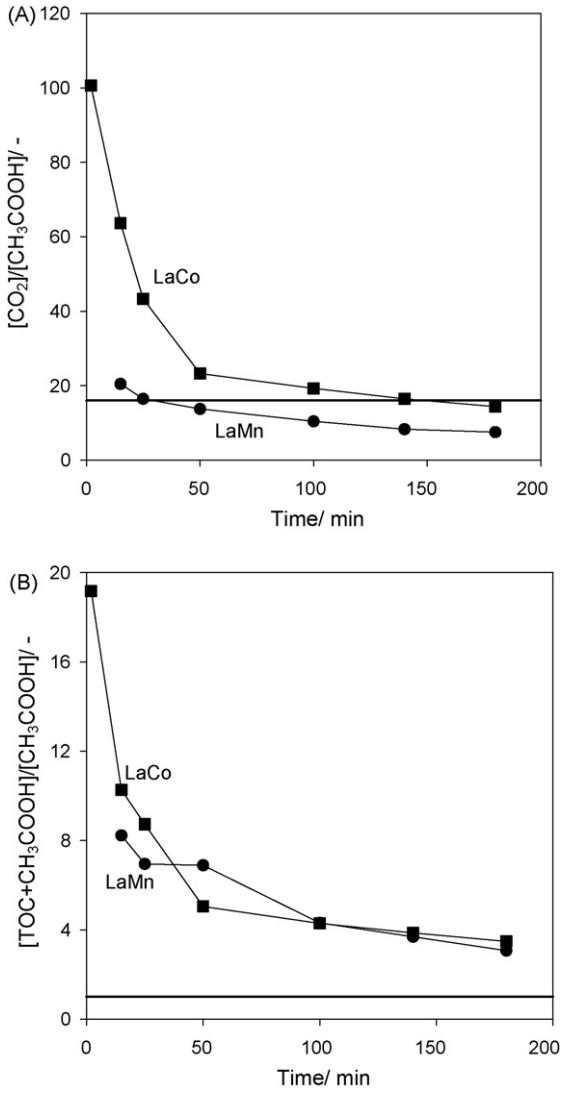

Fig. 6. Evolution of the $[CO_2]/[CH_3COOH]$ (A) and $TOC/[CH_3COOH]$ (B) ratios with the time in reaction for the LaCo and LaMn samples. Solid lines correspond to the theoretical value obtained in the case of a pure decarboxylation mechanism without acetic acid oxidation [11].

The results obtained with the Mn-based samples slightly differ from those obtained with the LaCo sample. The $[TOC + CH_3COOH]/[CH_3COOH]$ ratio still being higher than 1 (see Fig. 6B) also suggests incomplete oxidation with the initial stearic acid being converted into soluble shorter chain length carboxylic acids heavier than acetic acid. The $[CO_2]/[CH_3COOH]$ ratio lower than 16 at essentially all reaction times (see Fig. 6A) indicates however a CH_3COOH formation higher than predicted by the reaction path described in Eqs. (10) and (11). This result suggests that the oxidation of acetic acid is not as high in that case as it is with LaCo.

In conclusion, the LaCo and Mn-based samples seem to promote a recurrent decarboxylation process with high rate of CO_2 formation, especially visible for the LaCo sample. Some activity of the manganese-based samples for the C–C bond breaking mechanism is clearly suggested by the experimental results. Moreover, the lower concentration in acetic acid obtained for the LaCo sample at the end of the test compared to

that obtained for LaMn sample suggests that LaCo is more active than LaMn for the acetic acid oxidation.

4.2. Nature of the active oxygen

Significant differences in oxygen storage capacity were observed between the LaCo sample and the manganese-based samples. It was also observed that the lanthanum substitution by a divalent cation (Sr^{2+}) or by a quadrivalent cation (Ce^{4+}) leads to some change in OSC. Based on the results obtained in OSC, it is proposed that only Co^{3+}/Co^{2+} and Mn^{4+}/Mn^{3+} redox couples are active for the stearic acid oxidation reaction. In the case of the LaCo sample, a mineralization of 65.2% is obtained at the end of the reaction (Table 2). This mineralization degree corresponds to more than 80 times the oxygen amount generated by the reduction of all Co^{3+} into Co^{2+}. Similarly since only 30% of the manganese is in 4+ valency ($LaMnO_{3.15}$), the amount of oxygen consumed to mineralize 60.2% of the initial stearic acid (Table 2) corresponds to about 250 times of the oxygen generated by the reduction of all Mn^{4+} into Mn^{3+}. This suggests a catalytic mechanism with consumption of reactive O_2 molecules. Oxidation tests were also performed on nitrate salts (cobalt or manganese) dissolved in water at a concentration equivalent to the amount of transition metal lixiviated (Table 3) as catalyst. Dissolved cobalt and manganese do no present any homogeneous activity under these conditions, suggesting that the dissolved transition metal cannot be responsible for the mineralization observed during the test. Moreover, the drastic deactivation observed on the mineralization curves (Fig. 2) confirms the fact that transition metals in solution are rather inactive for the oxidation reaction. Based on these considerations, a catalytically activated mechanism can be proposed suggesting that the oxygen, dissolved in the solution and being adsorbed on the perovskite surface participates in the stearic acid oxidation.

As a matter of fact, the initial rate of oxidation (r_0 in Table 2) is found to be roughly dependant on the oxygen storage capacity of the fresh solids (OSC, Table 1) (Fig. 7). This relationship clearly suggests similarities between the CO oxidation mechanism and the stearic acid oxidation reaction. In the case of the CO oxidation reaction in the presence of gaseous oxygen, considered as a suprafacial reaction [44], Tascon et al. [45,46] proposed an oxidation mechanism in which the reaction between the dissociatively adsorbed oxygen (O^-) and the adsorbed CO results in the formation of surface carbonate species. This reaction is proposed as the rate determining step of the CO oxidation reaction. Nevertheless, because of the low reaction temperature, adsorbed molecular dioxygen (O_2^-) can also be considered as active species in low temperature oxidation reactions like CO oxidation reaction:

$$CO_{(g)} + O_{2(ads)}{}^- \rightarrow CO_{3(ads)}{}^- \quad (12)$$

Gaseous O_2 is adsorbed on low valency sites first (Co^{2+} or Mn^{3+}). Dissociation of the O_2 molecule (to form surface O^- species) on the surface is not necessary since O_2^- is a radical species and can react in its adsorbed form ($Co^{3+}O_2^-$). Then, the CO molecule reacts with adsorbed surface O_2^- species to form surface carbonate CO_3^- species. By decomposition, this carbonate leads to the desorption of CO_2, and formation of atomic oxygen [45,46]. The OSC experiment is performed under pulse regime. Then, after saturation of the surface by gaseous oxygen, pulses of CO pass through the catalyst at a constant temperature (180 °C in the present case).

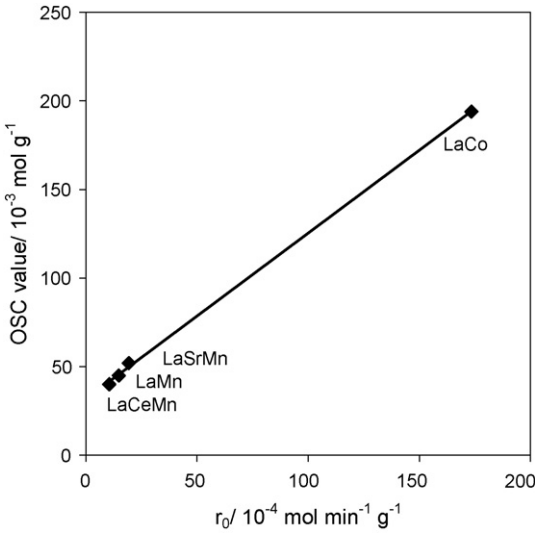

Fig. 7. Relationship between the initial rate of oxidation (R_0) and the oxygen storage capacity (OSC) obtained for the different catalysts.

Based on these considerations, the oxygen active in the stearic acid oxidation reaction may be considered to be any of the surface oxygen species (O_2^-, O^- and/or O^{2-}). As mentioned above, the reaction temperature is low which led us to suppose no or weak reactivity of lattice surface oxygen species (O^{2-}). Thus, stearic acid can react (after adsorption or not) with oxidized cobalt sites ($Co_{(surf)}{}^{3+}O_2^-$ for the LaCo sample) to form adsorbed carbonate species:

$$2Co_{(surf)}{}^{3+}O_2^- + C_{17}H_{35}COOH_{(ads)} \rightarrow Co_{(surf)}{}^{2+} + Co^{3+}CO_{3(ads)}{}^- + C_{16}H_{33}COOH_{(ads)} + H_2O_{(aq)} \quad (13)$$

The reduced sites ($Co_{(surf)}{}^{2+}$) can be reoxidized by adsorption of a dissolved O_2 molecule (Eq. (14)) for active site regeneration:

$$Co_{(surf)}{}^{2+} + O_{2(aq)} \rightarrow Co_{(surf)}{}^{3+}O_2^- \quad (14)$$

The reaction of the stearic acid molecule with surface O^- species, instead of adsorbed O_2^- species, cannot be completely excluded.

Similar mechanism can be proposed for the Mn-based samples, taking into account that reactive oxygen is located on 4+ valency sites, and that reaction with the stearic acid molecules leads to the formation of Mn^{3+} reduced sites which can be reoxidized following a process similar to the one described by Eq. (14). However, the higher concentration of Co^{3+} sites compared to Mn^{4+} sites (only 30% of the manganese is in 4+ valency) explains why LaCo presents a higher activity

in the stearic acid oxidation reaction. Since carbonates are formed during stearic acid oxidation, the possible implication of surface carbonate species as intermediate species during this reaction will be discussed in the next section.

4.3. Mechanism of deactivation

Results obtained for the stearic acid oxidation reaction reveals a strong deactivation of perovskite samples during reaction (Fig. 2). XRD analyses of the used samples showed the simultaneous formation of carbonate hydroxide hydrate together with the partial (manganese-based samples) or complete (LaCo sample) destruction of the perovskite structure (Fig. 4). Since carbonation cannot occur on dissolved lanthanum or transition metal species due to the acidic pH of the reaction medium, it may occur on the surface of the solid. It is interesting to note that a direct relationship comparable to the one found between the OSC value and the initial rate of oxidation (Fig. 7), was observed between the amounts of carbon accumulated (Table 2) and the OSC values measured at 200 °C (Table 1). This reveals that an increase in OSC (or transition metal reactivity) results in an increase in carbon accumulation on the catalyst (Fig. 8).

As mentioned above, the mechanism of stearic acid oxidation reaction forming CO_2 is suggested to lead to the formation of surface carbonate species (Eq. (13)) over perovskite samples. In the case of the CO oxidation reaction, Tascon et al. [45,46] proposed that the formation of the carbonate species is rate determining (Eq. (12)). Thereafter, carbonate species easily decompose and desorb, leading to no or small carbonation rate of the perovskite structure during this reaction. Taking into account the important extent of lanthanum carbonation during the stearic acid CWAO reaction, the rate determining step should be different for this reaction from that for the gas phase CO oxidation reaction. Under these considerations, it is possible to suppose that adsorbed CO_3^- species react with low valency cobalt site

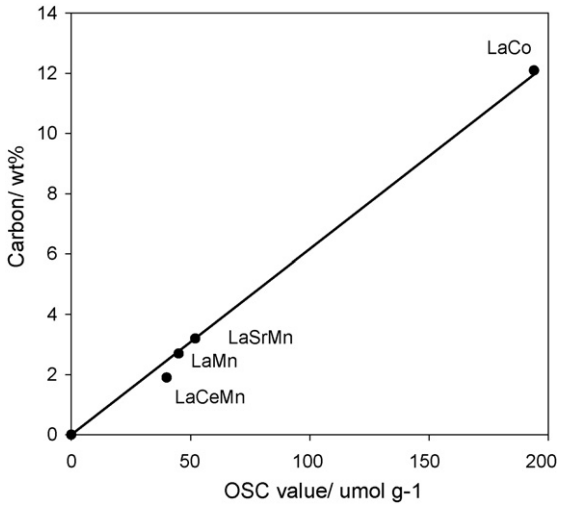

Fig. 8. Relationship between OSC value measured at 180 °C and the amount of carbon accumulated over the catalyst after stearic acid oxidation reaction at 200 °C.

(Co^{2+}) leading to the formation of stable doubly charged lattice carbonate species ($Co^{3+}CO_3^{2-}Co^{3+}$):

$$Co^{3+}CO_{3(ads)}^{-} + Co^{2+} \rightarrow Co^{3+}CO_3^{2-}Co^{3+} \quad (15)$$

These carbonates should obviously be more stable than surface carbonates so that the process described by Eq. (15) may efficiently compete with the desorption of CO_2.

The initial rate of CO_2 formation depends therefore directly on the reducibility of the transition metal. This is the reason why the rate of CO_2 formation is higher on the LaCo sample compared to the manganese-based samples. If the rate determining step of the stearic acid oxidation reaction is the rate of carbonate (CO_3^-) decomposition or CO_2 desorption, the surface concentration of CO_3^{2-} (Eq. (15)) should be higher for LaCo than it is for the manganese-based samples, leading to a higher lanthanum carbonation on the LaCo sample. These experimental results suggest a competition between desorption of the CO_2 (CO_2 is detected in the gas phase) and the carbonate incorporation in the structure (the solid is progressively converted into lanthanum carbonate hydroxide hydrate).

In the present work, lanthanum carbonation is then proposed to be the major cause of catalyst deactivation (decrease of the number of active sites). Moreover, the partial dissolution of the transition metal during reaction (Table 3, $TM_{sol} < 5\%$), leading to a decrease of the transition metal surface concentration, can also contribute to the decrease of the catalyst activity.

5. Conclusion

In this work, four perovskite samples synthesized by reactive grinding were tested for the stearic acid wet air oxidation (CWAO) reaction. It was observed that the nature of the transition metal strongly affects the initial activity of the sample. Significantly higher activity was obtained for the $LaCoO_3$ sample, compared to manganese-based perovskites. A mechanism, involving a progressive decarboxylation of the stearic acid molecule and the formation of CO_2 with a high selectivity, is proposed.

A direct relationship between the reducibility at low temperature (OSC value) and the initial catalytic activity of the sample was observed. This clearly showed that the reactivity of the redox couple (either Co^{3+}/Co^{2+} or Mn^{4+}/Mn^{3+}) is the parameter determining the initial activity of the sample. The $LaCoO_3$ sample, showing the highest oxygen storage capacity (measure of the most active oxygen), shows the highest initial activity for the reaction.

The proposed scheme of reaction involves the formation of stable bulk carbonates with lanthanum. The destruction of the perovskite structure by carbonate formation results in a decrease in stearic acid reaction sites concentration, and consequently in catalytic activity as suggests by the shape of the mineralization curves.

Acknowledgements

The financial contribution of the Natural Sciences and Engineering Council of Canada and Nanox Inc. (Québec,

Canada), through an industrial chair, are gratefully acknowledged.

References

[1] V.S. Mishra, V.M. Mahajani, J.B. Joshi, Ind. Eng. Chem. Res. 34 (1995) 2.
[2] A. Pintar, J. Levec, Chem. Eng. Sci. 47 (1992) 2395.
[3] S. Imamura, I. Fukuda, S. Ishida, Ind. Eng. Chem. Res. 27 (1988) 718.
[4] D. Duprez, F. Delanoe, J. Barbier Jr., P. Isnard, G. Blanchard, Catal. Today 29 (1996) 317.
[5] S. Hamoudi, F. Larachi, A. Sayari, J. Catal. 177 (1998) 247.
[6] S. Hamoudi, F. Larachi, G. Cerrella, M. Cassanello, Ind. Eng. Chem. Res. 37 (1998) 3561.
[7] S. Hamoudi, A. Sayari, K. Belkacemi, L. Bonneviot, F. Larachi, Catal. Today 62 (2000) 379.
[8] L. Oliviero, J. Barbier Jr., D. Duprez, H. Wahyu, J.W. Ponton, I.S. Metcalfe, D. Mantzavinos, Appl. Catal. B 31 (2001) 1.
[9] L. Oliviero, J. Barbier Jr., D. Duprez, A. Guerrero-Ruiz, B. Bachiller-Baeza, I. Rodriguez-Ramos, Appl. Catal. B 25 (2000) 267.
[10] H.T. Gomes, J.J.M. Orfao, J.L. Figueiredo, J.L. Faria, Ind. Eng. Chem. Res. 43 (2004) 1216.
[11] B. Renard, J. Barbier Jr., D. Duprez, S. Durecu, Appl. Catal. B 55 (2005) 1.
[12] W.F. Libby, Science 171 (1971) 499.
[13] D.W. Johnson Jr., P.K. Gallagher, F. Schrey, W.W. Rhodes, Ceram. Bull. 55 (1976) 520.
[14] D.W. Johnson Jr., P.K. Gallagher, G.K. Wertheim, E.M. Vogel, J. Catal. 48 (1977) 87.
[15] H. Arai, T. Yamada, K. Eguchi, T. Seiyama, Appl. Catal. 26 (1986) 265.
[16] G. Kremenic, J.M.L. Nieto, J.M.D. Tascon, L.G. Tejuca, J. Chem. Soc., Faraday Trans. 1 (1985) 939.
[17] T. Nitadori, T. Ichiki, M. Misono, Bull. Chem. Soc. Jpn. 61 (1988) 621.
[18] T. Seiyama, in: L.G. Tejuca, J.L.G. Fierro (Eds.), Properties and Application of Perovskite-Type Oxides, Dekker, New York, 1993, p. 215.
[19] T. Nitadori, M. Misono, J. Catal. 93 (1985) 459.
[20] L. Forni, C. Oliva, F.P. Vatti, M.A. Kandala, A.M. Ezerets, A.V. Vishniakov, Appl. Catal. B 7 (1996) 269.
[21] D. Ferri, L. Forni, Appl. Catal. B 16 (1998) 119.
[22] M. Yang, A. Xu, H. Du, C. Sun, C. Li, J. Hazard. Mater. B 139 (2007) 86.
[23] P. Morand-Fehr, G. Tran, INRA Prod. Anim. 14 (2001) 285.
[24] J. Shu, S. Kaliaguine, Appl. Catal. B 16 (1998) 303.
[25] S. Kaliaguine, A. Van Neste, V. Skabo, J.E. Gallot, M. Bassir, R. Muzychuk, Appl. Catal. A 209 (2001) 345.
[26] S. Kaliaguine, A. Van Neste, US Patent 6,017,504 (2000).
[27] D.W. Johnson Jr., P.K. Gallagher, F. Shrey, W.W. Rhodes, Ceram. Bull. 55 (1976) 520.
[28] P. Courty, H. Ajot, C. Marcilly, B. Delmon, Powder Technol. 7 (1973) 21.
[29] S. Royer, F. Berubé, S. Kaliaguine, Appl. Catal. A 282 (2005) 273.
[30] S. Royer, H. Alamdari, D. Duprez, S. Kaliaguine, Appl. Catal. B 58 (2005) 273.
[31] M. Crespin, W.K. Hall, J. Catal. 69 (1981) 359.
[32] L. Simono, F. Garin, G. Maire, Appl. Catal. 11 (1997) 167.
[33] S. Irusta, M.P. Pina, M. Menendez, J. Santamaria, J. Catal. 179 (1997) 400.
[34] B.C. Tofield, W.R. Scott, J. Solid State Chem. 10 (1974) 183.
[35] J.M.A. Van Roosmalen, E.H.P. Cordfunke, R.B. Helmholdt, H.W. Zandbergen, J. Solid State Chem. 110 (1994) 320.
[36] J. Barbier Jr., F. Delanoë, F. Jabouile, D. Duprez, G. Blanchard, P. Isnard, J. Catal. 177 (1998) 378.
[37] L. Oliviero, Thesis, Université de Poitiers, 2001.
[38] M. Alifanti, J. Kirchnerova, B. Delmon, Appl. Catal. A 245 (2003) 231.
[39] S. Royer, D. Duprez, S. Kaliaguine, J. Catal. 234 (2005) 364.
[40] L. Lisi, G. Bagnasco, P. Ciambelli, S. De Rossi, P. Porta, G. Russo, M. Turco, J. Solid State Chem. 146 (1999) 176.
[41] S. Ponce, M.A. Pena, J.L.G. Fierro, Appl. Catal. B 24 (2000) 193.
[42] K.S. Song, H.X. Cui, S.D. Kim, S.K. Kang, Catal. Today 47 (1999) 155.
[43] E. Sève, G. Antonini, Chem. Eng. J. 76 (2000) 179.
[44] R.J.H. Voorhoeve, J.P. Remeika Jr., L.E. Trimble, Ann. N. Y. Acad. Sci. 272 (1976) 3.
[45] J.M.D. Tascon, S. Mendioroz, L.G. Tejuca, Z. Phys. Chem. 124 (1981) 109.
[46] J.M.D. Tascon, S. Mendioroz, L.G. Tejuca, Z. Phys. Chem. 124 (1981) 249.